CrossMark

ORIGINAL PAPER

Tubular structured bacterial cellulose-based nitrite sensor: preparation and environmental application

Ya Zhang[1] · Zhifeng Zhou[1] · Fangfang Wen[1] · Kechun Yuan[1] · Jin Tan[1] · Zilan Zhang[1] · Honggui Wang[1,2]

Abstract Bacterial cellulose (BC) is a polysaccharide with tubular structure and can be produced by various species of bacteria particularly *Acetobacter xylinum*. It is a promising matrix for fabricating electrochemical devices as a mechanically strong, flexible, and biocompatible carbon-based material. In the present work, BC and graphene oxide (GO) composite was obtained simply via a mixing method. The scanning electron microscopy (SEM) and transmission electron microscopy (TEM) images showed that the BC nanofibers were imbedded in the GO wrinkled sheets. Raman spectra showed the D and G bans of BC-GO shifted towards higher frequency. Fourier transform infrared (FT-IR) spectroscopy spectra confirmed a hybrid structure was successfully obtained. Cyclic voltammetry (CV) results showed the BC-GO modified electrode had the best electrochemical activity. Nitrite could be oxidized using the BC-GO modified electrode in a wide range of pHs. The amperometric response result indicated the BC-GO modified GCE can be used to determine nitrite concentration in a wide linear range of 0.5 to 4590 μM with detection limit and sensitivity of 0.2 μM and 527.35 μA μM^{-1} cm^{-2}, respectively. The BC-GO nitrite sensor also showed good anti-interference and real sample analysis performances.

Introduction

During the past few years, carbon nanomaterials, including carbon nanotubes [1, 2], graphene (oxide) [3, 4], and cellulose [5], are one of the important matrixes for fabricating electrochemical devices. The reason is that most of the carbon materials are mechanically strong, flexible, and biocompatible. Among all the carbon nanomaterials, cellulose is receiving more and more attention because it is the most abundant, renewable, biodegradable natural polymer resource on earth, which can be found in plant cell walls [6], and also can be produced by some sea creatures (e.g., tunicates) [7] and bacteria (*Acetobacter xylinum*) [8]. It is a good matrix for fabricating composites and the resulting composites can be widely used as personal care products, paper, and packaging and food additives [8–11]. However, their properties, functionality, and uniformity cannot satisfy next generation of cellulose-based materials. This problem will be solved by extracting cellulose at the nanoscale.

There are two ways to obtain nanocellulose. Plant cellulose can convert to tubular structure under proper TEMPO-mediated oxidation [6]. Another way is biosynthesis of bacterial cellulose. Up to now, literatures about the plant cellulose-based sensors are available. For example, Zhou et al. has reported that hemoglobin entrapped in cyanoethyl cellulose film can be a good nitric oxide sensor [12]. Alizadeh's group has reported an optical Ni^{2+} sensor based on a triazene-1-oxide derivative, immobilized on the triacetyl cellulose membrane with a detection limit of 1.0×10^{-9} M [13]. Qi and coworkers have found that the electrically conductive film composed of carbon nanotubes (CNTs) and cellulose matrix can be used as

✉ Honggui Wang
  wanghg@yzu.edu.cn

1 School of Environmental Science and Engineering, Yangzhou University, Yangzhou 225127, Jiangsu, People's Republic of China

2 Key Laboratory of Prevention and Control of Biological Hazard Factors (Animal Origin) for Agrifood Safety and Quality, Ministry of Agriculture of China, Yangzhou University (26116120), Yangzhou 225009, Jiangsu, People's Republic of China

water sensors [14, 15]. Very recently, Kim et al. have reported a graphene and cotton cellulose nanocomposite with good mechanical, dielectric and electrical properties, which also shows good solvent-sensing performance [16]. However, to the best of our knowledge, there is little literature about bacterial cellulose nanocomposite fabricated sensor except a H_2O_2 sensor based on gold nanoparticle/bacterial cellulose nanocomposite [17]. As lots of literatures have confirmed, the plant cellulose can be a good candidate for sensing system, we have reasons to believe that bacterial cellulose (BC) can also be a promising matrix for fabricating sensors.

BC is a polysaccharide produced by various species of bacteria particularly *Acetobacter xylinum*. BC with abundant reactive hydroxyl groups (−OH) and tubular structure is becoming a promising biomatrix for environmental applications in photocatalysis [18–20], adsorption [21, 22], and antibacterial fields [23]. However, its electrochemical application has been confined by its low electrochemical activity. The way to solve this problem is to composite with other materials. Graphene oxide (GO), as another kind of carbon material, has gained a tremendous amount of recent research attention due to its excellent electrical, thermal, and mechanical performances. Besides, GO exhibits good solvent dispersity, which makes it a good candidate for fabricating composites. In recent years, a lot of works have been done on synthesis and application of the BC-GO nanocomposite [24–28]. For example, Feng et al. has obtained a highly flexible nanocomposite film of bacterial cellulose (BC) and graphene oxide (GO) by a vacuum-assisted self-assembly technique [25]. Nandgaonkar and coworkers have prepared a rGO/BC nanocomposite via a one-pot biosynthesis [26]. BC/GO and BC/GO/Ag antibacterial reagents have been investigated by Shao's and Chia's

groups, respectively [24, 27, 29]. Xiong and his colleagues have reported a 3D spherical carbonized BC/graphene nanocomposites with superior performances on oil and organic solvents adsorption [28].

In this work, bacterial cellulose and graphene oxide were obtained through a biosynthesis and modified Hummer's method, respectively. The BC-GO nanocomposite was prepared via an easy solution and sonication mixing method. Before electrochemical tests, the BC-GO was fully characterized. The BC-GO modified glassy carbon electrode (GCE) showed improved electrocatalytic activity for the oxidation of nitrite than that of GO and BC-based GCE. The BC-GO/GCE also had good anti-interference and real sample analysis performance.

Experimental

Materials

Acetobacter xylinum (ATCC 23767) was purchased from Guangdong Institute of Microbiology (China). Anhydrous citric acid, disodium phosphate (Na_2HPO_4), ethanol, graphite, magnesium sulfate ($MgSO_4$), monosodium phosphate (NaH_2PO_4), phosphoric acid (H_3PO_4), potassium phosphate (K_3PO_4), sodium chloride (NaCl), sulfuric acid (H_2SO_4), hydrogen peroxide (H_2O_2), sodium nitrate ($NaNO_3$), potassium permanganate ($KMnO_4$), sodium hydroxide (NaOH), sodium nitrite ($NaNO_2$), and other chemicals were purchased from Sinopharm Chemical Reagent Company. D-glucose, peptone, yeast extract, and other biochemicals were obtained from Sangon Biotech. All the reagents were of analytical grade or

Fig. 1 Schematic illustration of the BC-GO preparation and the proposed mechanism for nitrite detection
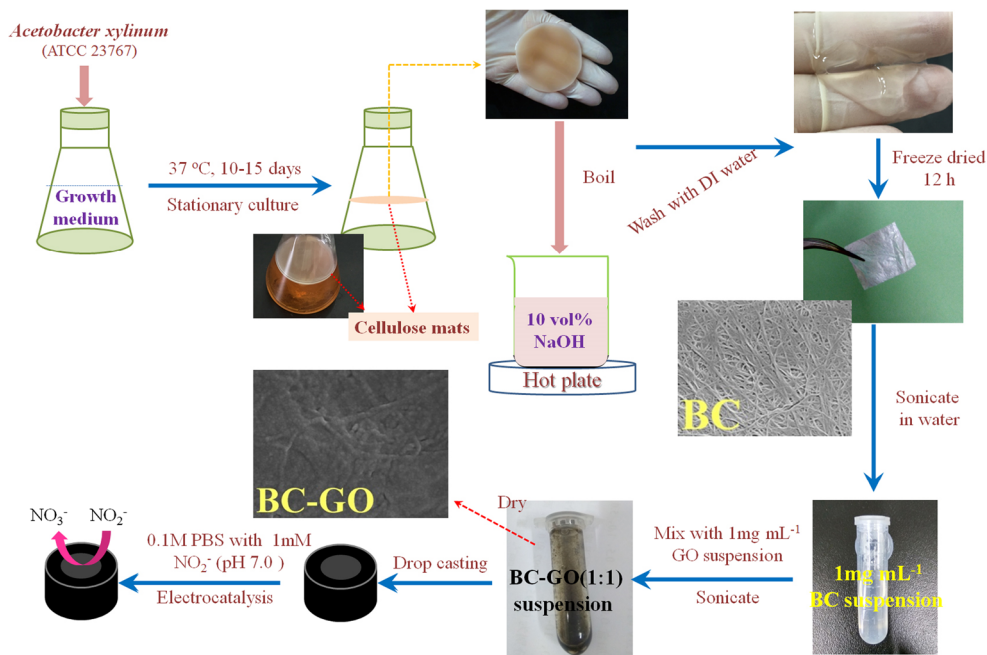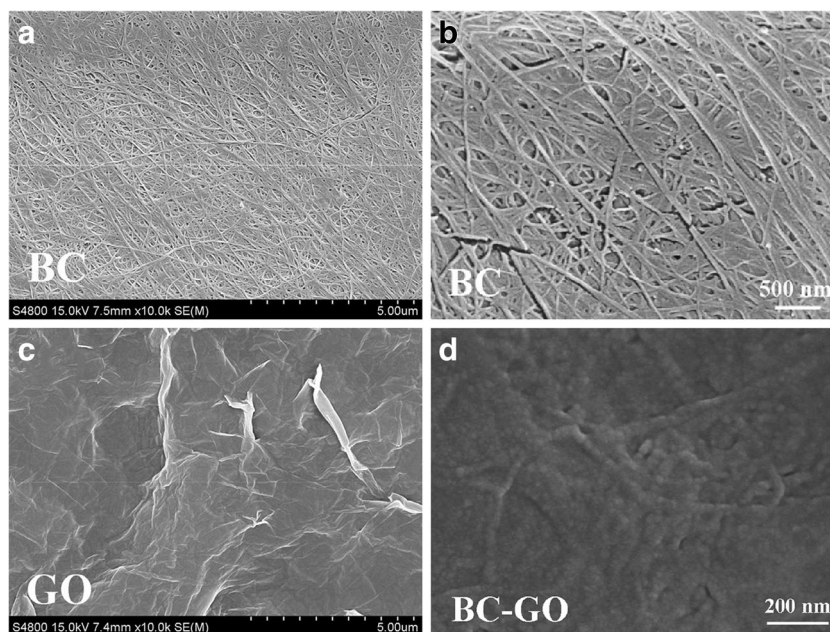
higher grade and used as received. All solutions were prepared with deionized (DI) water. Phosphate buffer solution (PBS, 0.1 M) with various pH ranges were prepared from 0.1 M H_3PO_4, NaOH, Na_2HPO_4, and NaH_2PO_4.

Synthesis of GO and biosynthesis of BC

GO was prepared by a modified Hummer's method as reported previously [30]. Briefly, 6.0 g graphite powders were mixed with 3.0 g $NaNO_3$ then cooled with ice. H_2SO_4 (138 mL) was added to the mixture and stirred uniformly. Then, 18.0 g $KMnO_4$ was added slowly to the mixture, controlling the reaction temperature below 20 °C. After that, the mixture was stirred and warmed to 35 °C for 30 min. Next, 250 mL DI water was added slowly to the mixture while maintaining the reaction temperature at 98 °C for 15 min. The mixture was then cooled down by adding additional 420 mL DI water and 3 mL H_2O_2 (30%). After cooling in air, the black precipitate was collected by centrifugation,

washed three times with distilled water and ethanol, and then dried in an oven at 65 °C for 10 h. To prepare the 1 mg mL^{-1} GO suspension, 1 mg GO was dispersed in 1 mL DI water with the help of sonication.

To get cellulose mats shown in Fig. 1, *A. xylinum* (ATCC 23767) was inoculated in sterilized growth medium. The medium (1 L) was composed of 20 g of D-glucose, 5 g of yeast extract, 1.15 g of anhydrous citric acid, 5.7 g of $MgSO_4$, 5.0 g of peptone, 2.5 g of NaCl, 4.5 g of Na_2HPO_4, 0.75 g of K_3PO_4, and 1 vol% ethanol (96%). The bacteria were plated on medium. After 3 days, the bacteria were scraped from flat plate, suspended in growth medium, and then transferred to a 250 mL flask with 200 mL growth medium. After 10 to 15 days of growth at 28 °C, the mats were harvested. Then the mats were cut into 1 cm^3 pieces and boiled repeatedly in distilled water until no residual growth medium could be detected. Then the mats were boiled twice in a 0.1 mol/L concentrated NaOH (1.5 L) for 20 min. Finally, the pieces were rinsed with DI water until pH ≈ 7. The transparent bacterial

Fig. 3 TEM images of (**a**) *BC* and (**b**) *BC-GO* (inset: BC-GO in low resolution)
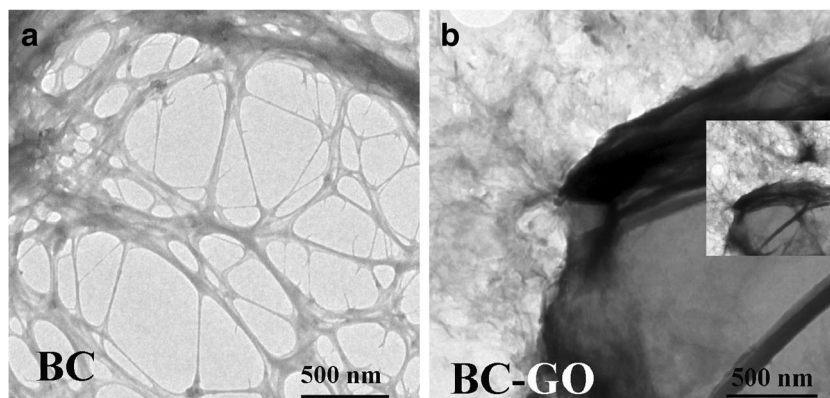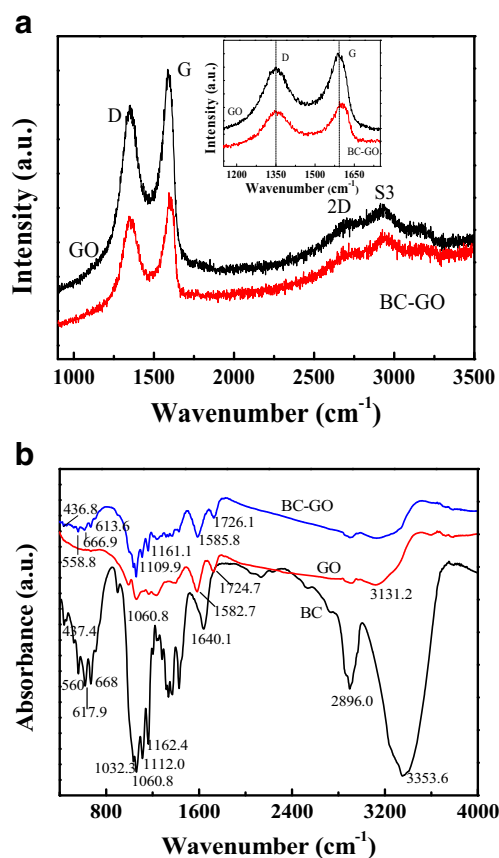
Fig. 4 (a) Raman spectra of GO and BC-GO, (b) FT-IR of BC, GO, and BC-GO

cellulose (BC) as shown in Fig. 1 was obtained. Before electrochemical application, the BC was freeze dried for 48 h. The BC white papers with carbon nanotube-like structure were obtained.

Preparation of BC-GO modified GC electrode

Preparation of BC-GO modified GC electrode is expressed in Fig. 1: step 1: 1 mg BC paper was dispersed in 1 mL DI water and sonicated with a high-power ultrasonic tip (Y-92-N, Ningbo Scientz Biotechnology Co., Ltd) to form a uniform 1 mg mL^{-1} suspension; step 2: certain amount of 1 mg mL^{-1} GO was mixed with the 1 mg mL^{-1} BC suspension to form the 1 mg mL^{-1} BC-GO composite suspensions; step 3: 5 μL BC-GO suspension was drop-casted onto the surface of clean glassy carbon (GC) electrode to prepare the BC-GO modified GC electrode; step 4: the BC-GO modified GC electrode was used to determine nitrite in a 0.1 M PBS with various concentrations of nitrite.

Instruments

Scanning electron microscopy (SEM) images were obtained on an S-4800 field-emission scanning electron microanalyzer

(Hitachi, Japan). Transmission electron microscopy (TEM) was recorded on a Tecnai G2F30S-TWIN transmission electron microscope. Raman and Fourier transform infrared (FT-IR) spectra were measured using a Micro-Raman spectrometer (Renishaw in Via, U.K) (532.8 nm) and a Cary 610/670 microscope (Varian, US), respectively. The nitrite concentrations have been confirmed by ion chromatography (ICS2100, Dionex). All electrochemical experiments were performed on a CHI 660 D electrochemical workstation (CHI). The three-electron system contains a modified GC (3 mm diameter, CHI), a platinum wire counter electrode, and a saturated calomel reference electrode (SCE). The solution pH values were determined using a PHS-3C pH meter.

Results and discussions

Characterization of BC-GO

Before electrochemical tests, the BC-GO composite is fully characterized by SEM, TEM, Raman, and FT-IR spectra. The SEM images of BC, GO, and BC-GO composite are investigated and shown in Fig. 2. As can be seen in Fig. 2a and b, the as-obtained
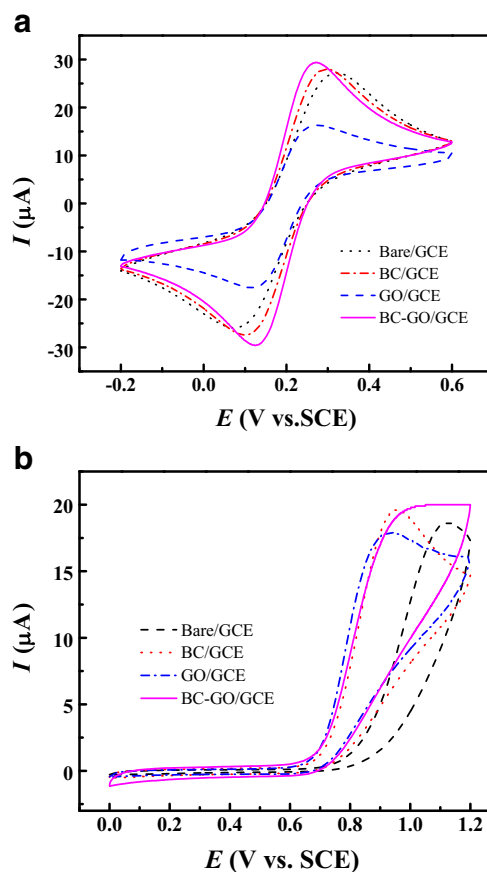
Fig. 5 Electrochemical activity of bare *GCE*, *BC*, *GO*, and *BC-GO* modified *GCE* in a 5.0 mM [Fe(CN)$_6$]$^{3-/4-}$ (1:1) containing 0.1 M KCl (**a**) and pH 7.0, 0.1 M PBS with 1 mM nitrite (**b**), respectively
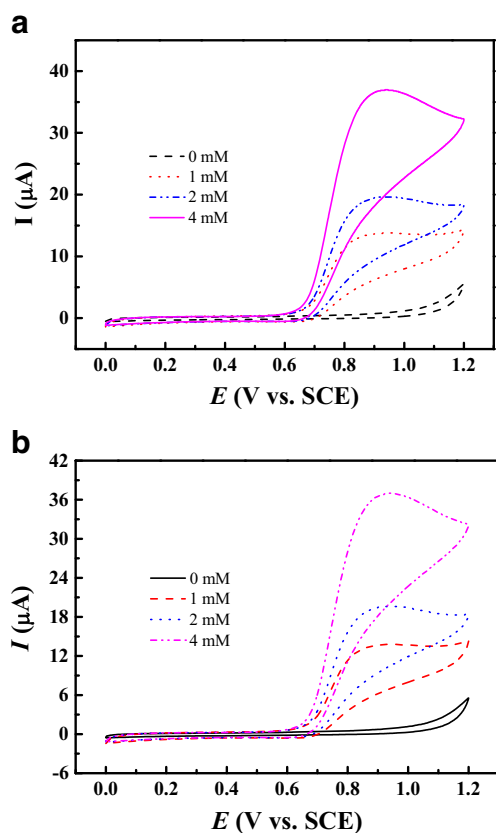
Fig. 6 CVs of BC-GO modified GCE in a pH 7.0, 0.1 M PBS without and with various concentrations of nitrite, at a scan rate of 50 mV s^{-1}. **a** Low to high concentrations and **b** high to low concentrations

BC displays a uniform multi-walled carbon nanotube-like structure with a diameter of 20 to 30 nm while the GO looks like a wrinkled sheet (Fig. 2c), which is a typical structure of GO as reported in literature [4]. When the BC suspension is mixed with GO suspension, both structures are retained. It can be seen clearly in Fig. 2d that the nanofibers of BC are imbedded in the wrinkled sheet. TEM images of BC (Fig. 3a) and BC-GO (Fig. 3b) are in accordance with the results of SEM.

The BC-GO composite is further confirmed by Raman and FT-IR spectra. Figure 4a displays the Raman spectra of GO and BC-GO nanocomposite. Both spectra show similar shape. Two main peaks at about 1300 and 1600 cm^{-1} are D and G bands, respectively. Another two weak peaks at about 2650 and 2900 cm^{-1} are 2D and S3 bands, respectively. The presence of 2D and S3 bands ascribe to an out-of-plane vibration mode and the lattice disorders [31]. There are two differences between GO and BC-GO nanocomposite. It can be seen clearly in the inset of Fig. 4a that both D and G bands shift towards higher frequencies in the BC-GO spectrum. In addition, the intensity ratio of D/G decreases compared to that of GO (0.871 to 0.857), which indicates an increase in the average size of sp^2 domains [32]. This may be caused by the adding of BC in the GO links the edges of GO and results in a larger size. Figure 4b shows the FT-IR spectra of BC, GO, and BC-GO. In

the case of BC, the peak at 3353.6 cm^{-1} corresponds to the intramolecular hydrogen bond for 3O···H–O5 and the hydroxyl groups [33]. The peak at 2896.0 and 1640.1 cm^{-1} are attributed to C–H stretching and –CO–NH– stretching vibration, respectively [27]. In the C–O stretching vibration region (1200–1000 cm^{-1}), the band at 1162.4, 1112.0, 1068.0, and 1032.3 cm^{-1} can be assigned to the vibrations of C1–O–C4, C2–O2H, C3–O3H, and C6H2–O6H, respectively [25]. In the spectrum of GO, the board peak around 3100–3400 cm^{-1} corresponds to the stretching vibration of hydroxyl groups. The peaks appear at 1724.7, 1582.6, and 1068.0 cm^{-1} can be assigned to stretching vibrations of C = O carboxylic moieties, −COOH and C–O, respectively [25, 27]. For the BC-GO nanocomposite, it contains the typical C–O stretching vibration region of BC and the characteristic stretching vibrations of C = O carboxylic moieties (1726.1 cm^{-1}) of GO, which reveals a hybrid structure.

Electrochemical activity and electrocatalytic performance

Cyclic voltammetry (CV) technique is used to evaluate the electrochemical activities of BC, GO, and BC-GO modified
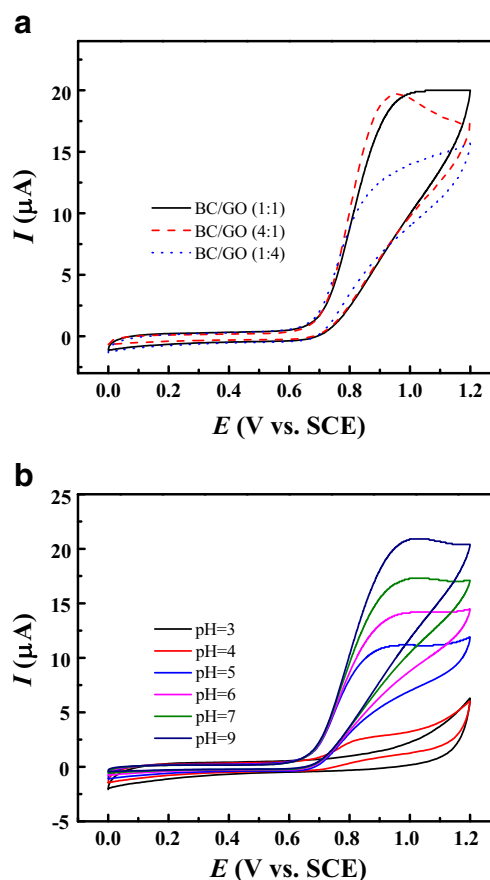

Fig. 7 **a** CVs of BC-GO modified GCE with various BC/GO ratios in a pH 7.0, 0.1 M PBS. **b** CVs of BC-GO nanocomposite modified GCE in a 0.1 M PBS with 1 mM nitrite at different solution pHs (pH 3.0–9.0). Scan rate, 50 mV s^{-1}
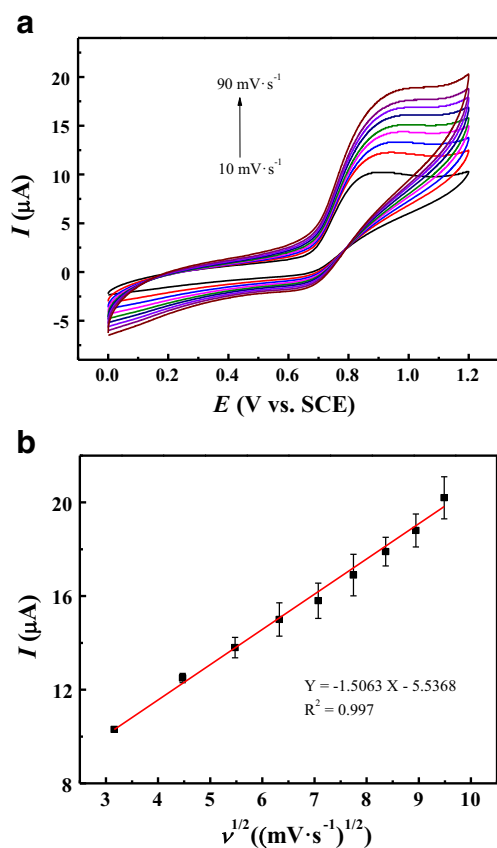
Fig. 8 **a** CVs of the BC-GO nanocomposite modified GCE in a 0.1 M PBS solution with 1 mM nitrite (pH 7.0) at different scan rates (10–90 mV s^{-1}). **b** The relationship between the oxidation peak current I_p and the scan rate $\upsilon^{1/2}$

GC electrodes. Figure 5a displays the electrochemical activity of the bare, BC, GO, and BC-GO modified GCE examined in a 0.1 M KCl containing 5.0 mM [Fe(CN)$_6$]$^{3-}$/$^{4-}$ (1:1) by CVs at a scan rate of 50 mV s^{-1}. As shown in Fig. 5a, for bare GCE, a couple of redox peaks appears with peak-to-peak separation (ΔEp) of 232 mV while the modified electrodes have smaller ΔEp of 183, 148, and 139 mV for BC, GO, and BC-GO modified GCE, respectively. The decrease of the ΔEp indicates BC-GO modified electrode has good reversibility in the electrochemical reaction process. In addition, the higher peak current response also reveals the higher electrical conductivity of BC-GO modified electrode. As for the GO modified electrode, the peak currents of redox peaks decreased obviously may be attributed to the negatively charged carboxyl group on GO surface [34]. Figure 5b shows the CVs of BC, GO, and BC-GO modified GC electrodes in a pH 7.0 PBS with 1 mM nitrite at a scan rate of 50 mV s^{-1}. Both BC and bare GC electrodes display poor electrochemical activity. The electrochemical activity of GO is better than that of BC. For BC-GO modified GC electrode, electrochemically active surface areas increase sharply. This result indicates BC-GO modified GCE has the best electrochemical activity, which is in accordance with the result shown in Fig. 5a.

As N-nitrosamines have potential carcinogenic effects and can form in the presence of nitrite, nitrite is selected as a target pollutant to investigate the electrochemical performance of BC-GO modified GCE. Figure 6a shows the CVs of the BC-GO modified GC electrode in a pH 7.0 PBS with various concentrations (0 ~ 4 mM) of nitrite at a scan rate of 50 mV s^{-1}. As displayed in Fig. 6a, no oxidation peak is available without nitrite and the current of the oxidation peak (~0.90 V) increases with increasing concentration of nitrite. This result indicates that nitrite could be oxidized by the BC-GO. In order to confirm the reversibility of the sensor, the CV of BC-GO modified GCE in a pH 7.0 PBS from high to low concentration is also presented. As displayed in Fig. 6b, the current of the oxidation peak (~0.90 V) decreases with decreasing concentration of nitrite. This result suggests that the BC-GO modified GCE has a good reversibility. To fully understand the electrocatalytic oxidation of nitrite by BC-GO modified GC electrode, various factors (molar ration of BC/GO, scan rates, solution pH) influencing nitrite oxidation are considered. The molar ration of BC/GO is also considered and shown in Fig. 7a. As displayed in Fig. 7a, the molar ration of BC/GO = 1:1 is best. Therefore, BC/GO = 1:1 is used in the following experiments unless otherwise stated. The
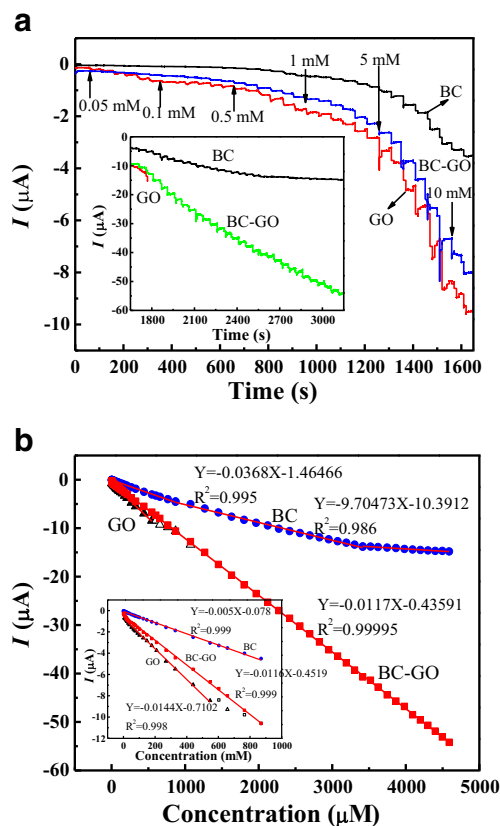
Fig. 9 **a** Amperometric response curves of *BC*, *GO*, and *BC-GO* modified GCE in a 0.1 M PBS (pH 7.0). **b** Plot of response currents vs. nitrite concentrations. Polarization potential, 1.0 V

Table 1 Performance comparison of BC-GO with other matrix for nitrite sensors

Electrode material	Linear range / μM	Detection limit / μM	Reference
ERGO-Pd	4–840	1	[4]
TOSC-MoS$_2$	6–3140, 3140–4200	2.0	[6]
CR-GO/GCE	8.9–167	1.0	[32]
MWNT-PAMAM-Chit	0.1–29, 29–254	0.01	[37]
Au–Pd/rGO	0.05–1000	0.02	[38]
Fe$_3$O$_4$/rGO/GCE	1–210	0.3	[39]
PANI-MoS$_2$/GCE	4.0–4834	1	[40]
Fe$_3$O$_4$/MoS$_2$	1–2630	0.5	[41]
Ag-AFS	1–16,000	0.07	[42]
GR-MWCNTs/FeNPs	0.1–1680	0.076	[43]
PEDOT	1–1000	1	[44]
BG-GO/GCE	0.5–4590	0.2	This work

influence of solution pH on the nitrite electrochemical oxidation is considered in the pH range of 3.0 to 9.0. As shown in Fig. 7b, when the solution pH is lower than 4.0, no obvious oxidation peak could be observed. While the anodic peak current increases sharply with increasing the solution pH value from 5.0 to 9.0, it should be noted here that the area of CV curves changes a little in the pH ranges of 5.0 to 9.0, which indicates the electrochemical activity of the BC-GO modified GCE remain unchanged. It is reported that nitrite oxidation is a proton independent catalytic step [35, 36], which means the change of anodic peak current is attributed to a kinetic reason. This result suggests that the BC-GO modified GCE can be used in a wide pH ranges. For practical purpose, the working pH is set at 7 unless otherwise stated. The effect of scan rates on the electrocatalytic oxidation of nitrite is investigated and presented in Fig. 8a. When the scan rates increase from 10 to 90 mV s^{-1}, the currents of the oxidation peak at about 0.90 V increase accordingly. The relationship between the oxidation peak current I_p and the square root of scan rate is recorded in Fig. 8b. From Fig. 8b, the oxidation peak currents are proportional to the square root of scan rate ($Y = -1.5063X - 5.5368$, $R^2 = 0.997$), which suggests that the nitrite oxidation process is diffusion control.

Amperometric determination

Amperometric technology is used to determine the parameters, including linear range, detection limit, and sensitivity, of the BC, GO, and BC-GO-based nitrite sensors. Figure 9a shows the typical amperometric responses of the BC, GO, and BC-GO-based nitrite sensors upon successive addition of 5.0×10^{-5}, 1.0×10^{-4}, 5.0×10^{-4}, 1.0×10^{-3}, 5.0×10^{-3}, and 1.0×10^{-2} M of nitrite in a 0.1 M PBS (pH 7.0) at an

applied potential of 1.0 V. As shown in Fig. 9a, all the three sensors display certain response to the successive injection of nitrite solution. Figure 9b is the corresponding relationships between the response currents of the BC, GO, and BC-GO-based nitrite sensors and the concentrations of nitrite in Fig. 9a. It is obvious that the BC-GO-based nitrite sensor has the widest linear range. The response currents at the BC-GO modified GCE are proportional to the concentration of nitrite in the range of 0.5–4590 μM ($R^2 = 0.99995$), which is wide enough for practical application (drinking water limit quantity postulated by the WHO is 43 μM) [4]. The corresponding sensitivity of the BC-GO modified GCE is 527.35 μA μM^{-1} cm^{-2}. A low detection limit of 0.2 μM nitrite is determined at the signal-to-noise (S/N) ratio of 3, while the repetitive response of the detection was obtained with a relative standard deviation of about 2.6%. The performances of nanocellulose, graphene (oxide)-based nitrite sensors, and the works about nitrite sensing our group have done are summarized in Table 1 [4, 6, 32, 37–44]. As indicated in Table 1, the performance of the BC-GO modified GCE is quite comparable to most of the nitrite sensors cited.
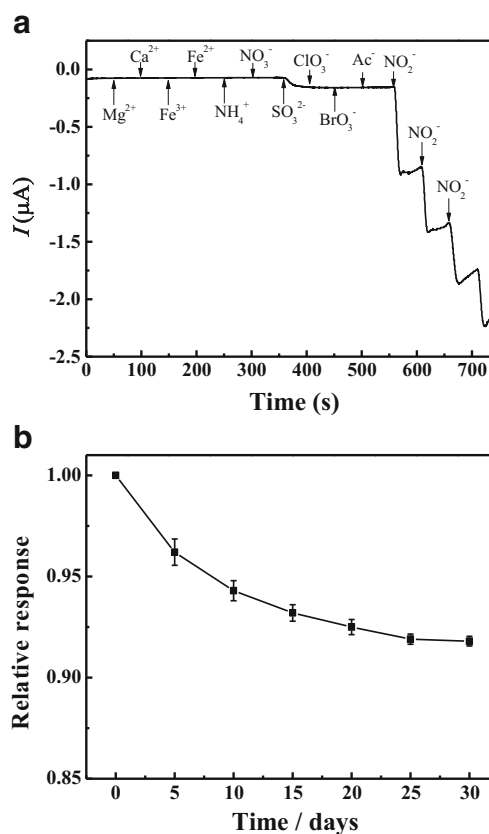
Fig. 10 **a** Response of the BC-GO sensor to various compounds at concentrations of 2.0×10^{-3} M (40 μL). Electrolyte, 0.1 M PBS, pH 7.0. Polarization potential, 1.0 V. **b** Stabilities of the BC-GO modified GCE stored at 4 °C in 0.1 M PBS, pH 7.0. Measurements for 1 mM nitrite were carried out in a pH 7.0 0.1 M PBS aqueous solution at 1.0 V

Table 2 Experimental verification of the BC-GO nitrite sensor on real samples

Sample	Theoretical [nitrite] / μM	Practical [nitrite] / μM	Recovery / %	RSD / % ($n = 3$)
Tap water	40.00	38.87	97.35	2.69
	150.00	147.36	98.17	1.97
Pond water	40.00	41.36	103.17	2.15
	150.00	147.09	98.11	2.33

Interference study, stability, and real sample analysis

The selectivity of BC-GO sensor is investigated by detecting 20 μM nitrite with the addition of various interference species into a 0.1 M PBS (pH = 7). Concentration of interfering ions is fixed to 2 mM, which is 100-fold that of nitrite. As shown in Fig. 10a, the determination of 20 μM nitrite cannot be interfered by the presence of the ions, including Mg^{2+}, Ca^{2+}, Fe^{3+}, Fe^{2+}, NH_4^+, NO_3^-, ClO_3^-, BrO_3^-, and Ac^-, which indicates that the BC-GO sensor owns a good selective recognition for nitrite. However, the presence of SO_3^{2-} exhibits obvious interference. This is attributed to the presence of Fe^{3+}, which can oxidize SO_3^{2-} into SO_4^{2-} [45].

Stability of the BC-GO sensor stored at 4 °C in 0.1 M PBS (pH = 7) aqueous solution is investigated by measuring the current responses every 5 days and shown in Fig. 10b. As displayed in Fig. 10b, the response currents of the BC-GO sensor decrease gradually to ~91% of the initial values after being stored for 30 days. The relative standard deviation (RSD) of the BC-GO sensor is 2.75%. The better storage stability of the electrode in pH 7.0, 0.1 M PBS aqueous solution indicates that BC-GO is stable in neutral condition.

Real sample (tap and pond water) analysis is presented and compared in Table 2. Superior recovery results can be achieved for both tap water (97.35% in lower concentration and 98.17% in higher concentration) and river water (103.17% in lower concentration and 98.11% in higher concentration) samples. Three measurements are performed at each concentration and the RSD of the proposed nitrite sensor for real samples analysis varies from 1.97 to 2.69%, which indicates the BC-GO sensor has the required accuracy for nitrite determination and could be efficiently used for real sample analysis.

Conclusions

In this work, a bacterial cellulose-graphene oxide (BC-GO) biosensor is successfully fabricated. It is confirmed by the results of SEM and TEM that the wrinkled sheet-like GO works as a substrate and the carbon nanotube-like BC grown on the surface of GO can increase the sp^2 domains of GO. As a key element of sensor, the BC-GO nanocomposite combines the advantages of BC and GO can make more efficient signal transformation between the target pollutants and the transducer. The BC-GO modified GCE can be used for the determination of nitrite in tap and pond water with appreciable accuracy and good selectivity. The work will not only enlarge the environmental application of BC, but also open up a new platform for fabricating BC-based electrochemical devices.

References

1. Ahmed SR, Kim J, Suzuki T, Lee J, Park EY (2016) Enhanced catalytic activity of gold nanoparticle-carbon nanotube hybrids for influenza virus detection. Biosens Bioelectron 85:503–508

2. Eguílaz M, Gutierrez F, González-Domínguez JM, Martínez MT, Rivas G (2016) Single-walled carbon nanotubes covalently functionalized with polytyrosine: A new material for the development of NADH-based biosensors. Biosens Bioelectron 86:308–314

3. Zhang Y, Wen FF, Jiang Y, Wang L, Zhou CH, Wang HG (2014) Layer-by-layer construction of caterpillar-like reduced grapheneoxide–poly(aniline-co-o-aminophenol)–Pd nanofiber on glassycarbon electrode and its application as a bromate sensor. Electrochim Acta 115:504–510

4. Zhang Y, Zhao YH, Yuan SS, Wang HG, He CD (2013) Electrocatalysis and detection of nitrite on a reduced graphene/Pd nanocomposite modified glassy carbon electrode. Sensors Actuators B Chem 185:602–607

5. Evans BR, O'Neill HM, Malyvanh VP, Lee I, Woodward J (2003) Palladium-bacterial cellulose membranes for fuel cells. Biosens Bioelectron 18:917–923

6. Wang HG, Wen FF, Chen YJ, Sun T, Meng Y, Zhang Y (2016) Electrocatalytic determination of nitrite based on straw cellulose/molybdenum sulfide nanocomposite. Biosens Bioelectron 85:692–697

7. Favier V, Chanzy H, Cavaille JY (1995) Polymer nanocomposites reinforced by cellulose whiskers. Macromolecules 28:6365–6367

8. Svensson A, Nicklasson E, Harrah T, Panilaitis B, Kaplan DL, Brittberg M, Gatenholm P (2005) Bacterial cellulose as a potential scaffold for tissue engineering of cartilage. Biomaterials 26:419–431

9. Khalil HPSA, Davoudpour Y, Islam MN, Mustapha A, Sudesh K, Dungani R, Jawaid M (2014) Production and modification of nanofibrillated cellulose using various mechanical processes: a review. Carbohydr Polym 99:649–665

10. Shatkin JA, Wegner TH, Bilek EM, Cowie J (2014) Market projections of cellulose nanomaterial-enabled products-Part 1: Applications. TAPPI J 13:9–16

11. Shi ZJ, Zhang Y, Phillips GO, Yang G (2014) Utilization of bacterial cellulose in food. Food Hydrocoll 35:539–545

12. Jia SS, Fei JJ, Zhou JP, Chen XM, Meng JQ (2009) Direct electrochemistry of hemoglobin entrapped in cyanoethyl cellulose film and its electrocatalysis to nitric oxide. Biosens Bioelectron 24:3049–3054

13. Alizadeh K, Rezaei B, Khazaeli E (2014) A new triazene-1-oxide derivative, immobilized on the triacetyl cellulose membrane as an optical Ni^{2+} sensor. Sensors Actuators B Chem 193:267–272

14. Qi HS, Liu JW, Deng YH, Gao SL, Mäder E (2014) Cellulose fibres with carbon nanotube networks for water sensing. J Mater Chem A 2:5541–5547

15. Qi HS, Mäder E, Liu JW (2013) Unique water sensors based on carbon nanotube–cellulose composites. Sensors Actuators B Chem 185:225–230

16. Kafy A, Sadasivuni KK, Akther A, Min SK, Kim J (2015) Cellulose/graphene nanocomposite as multifunctional electronic and solvent sensor material. Mater Lett 159:20–23

17. Zhang TJ, Wang W, Zhang DY, Zhang XX, Ma YR, Zhou YL, Qi LM (2010) Biotemplated synthesis of gold nanoparticle–bacteria cellulose nanofiber nanocomposites and their application in biosensing. Adv Funct Mater 20:1152–1160

18. Chen MY, Kang HL, Gong YM, Guo J, Zhang H, Liu RG (2015) Bacterial cellulose supported gold nanoparticles with excellent catalytic properties. ACS Appl Mater Interfaces 7:21717–21726

19. Sun DP, Yang JZ, Wang X (2010) Bacterial cellulose/TiO_2 hybrid nanofibers prepared by the surface hydrolysis method with molecular precision. Nanoscale 2:287–292

20. Yang JZ, Yu JW, Fan J, Sun DP, Tang WH, Yang XJ (2011) Biotemplated preparation of CdS nanoparticles/bacterial cellulose hybrid nanofibers for photocatalysis application. J Hazard Mater 189:377–383

21. Nata IF, Sureshkumar M, Lee CK (2011) One-pot preparation of amine-rich magnetite/bacterial cellulose nanocomposite and its application for arsenate removal. RSC Adv 1:625–631

22. Zhou YM, Fu SY, Zhang LL, Zhan HY, Levit MV (2014) Use of carboxylated cellulose nanofibrils-filled magnetic chitosan hydrogel beads as adsorbents for Pb (II). Carbohydr Polym 101:75–82

23. Janpetch N, Saito N, Rujiravanit R (2016) Fabrication of bacterial cellulose-ZnO composite via solution plasma process for antibacterial applications. Carbohydr Polym 148:335–344

24. Chook SW, Chia CH, Zakaria S, Ayob MK, Huang NM, Neoh HM, Jamal R (2015) Antibacterial hybrid cellulose–graphene oxide nanocomposite immobilized with silver nanoparticles. RSC Adv 5:26263–26268

25. Feng YY, Zhang XQ, Shen YT, Yoshino K, Feng W (2012) A mechanically strong, flexible and conductive film based on bacterial cellulose/graphene nanocomposite. Carbohydr Polym 87:644–649

26. Nandgaonkar AG, Wang QQ, Fu K, Krause WE, Wei QF, Gorga R, Lucian A (2014) A one-pot biosynthesis of reduced graphene oxide (RGO)/bacterial cellulose (BC) nanocomposites. Green Chem 16:3195–3201

27. Shao W, Liu H, Liu XF, Wang SX, Zhang R (2015) Anti-bacterial performances and biocompatibility of bacterial cellulose/graphene oxide composites. RSC Adv 5:4795–4803

28. Wan YZ, Zhang FS, Li CZ, Xiong GY, Zhu Y, Luo H (2015) Facile and scalable production of three-dimensional spherical carbonized bacterial cellulose/graphene nanocomposites with a honeycomb-like surface pattern as potential superior absorbents. J Mater Chem A 3:24389–24396

29. Shao W, Wang SX, Liu H, Wu JM, Zhang R, Min HH, Huang M (2016) Preparation of bacterial cellulose/graphene nanosheets composite films with enhanced mechanical performances. Carbohydr Polym 138:166–171

30. Allen MJ, Tung VC, Kaner RB (2010) Honeycomb carbon: a review of graphene. Chem Rev 110:132–145

31. Cuong TV, Pham VH, Tran QT, Hahn SH, Chung JS, Shin EW, Kim EJ (2010) Photoluminescence and Raman studies of graphene thin films prepared by reduction of graphene oxide. Mater Lett 64:399–401

32. Mani V, Periasamy AP, Chen SM (2012) Highly selective amperometric nitrite sensor based on chemically reduced graphene oxide modified electrode. Electrochem Commun 17:75–78

33. Oh SY, Yoo D, Shin Y, Kim HC, Kim HY, Chung YS, Park WH, Youk JH (2005) Crystalline structure analysis of cellulose treated with sodium hydroxide and carbon dioxide by means of X-ray diffraction and FTIR spectroscopy. Carbohydr Res 340(15):2376–2391

34. Li JH, Kuang DZ, Feng YL, Zhang FX, Xu ZF, Liu MQ (2012) A graphene oxide-based electrochemical sensor for sensitive determination of 4-nitrophenol. J Hazard Mater 201:250–259

35. Pournaghi-Azar MH, Dastangoo H (2004) Electrocatalytic oxidation of nitrite at an aluminum electrode modified by a chemically deposited palladium pentacyanonitrosylferrate film. J Electroanal Chem 567:211–218

36. Afkhami A, Madrakian T, Ghaedi H, Khanmohammadi H (2012) Construction of a chemically modified electrode for the selective determination of nitrite and nitrate ions based on a new nanocomposite. Electrochim Acta 66:255–264

37. Chen QP, Ai SY, Zhu XB, Yin HS, Ma Q, Qiu YY (2009) A nitrite biosensor based on the immobilization of Cytochrome con multiwalled carbon nanotubes–PAMAM–chitosan nanocomposite modified glass carbon electrode. Biosens Bioelectron 24:2991–2996

38. Li SS, Hu YY, Wang AJ, Weng XX, Chen JR, Feng JJ (2015) Simple synthesis of worm-like Au–Pd nanostructures supported on reduced graphene oxide for highly sensitive detection of nitrite. Sensors Actuators B Chem 208:468–474

39. Teymourian H, Salimi A, Khezrian S (2013) Fe_3O_4 magnetic nanoparticles/reduced graphene oxide nanosheets as a novel electrochemical and bioeletrochemical sensing platform. Biosens Bioelectron 49:1–8

40. Zhang Y, Chen P, Wen FF, Huang C, Wang HG (2016) Construction of polyaniline/molybdenum sulfide nanocomposite: characterization and its electrocatalytic performance on nitrite. Ionics 22:1095–1102

41. Zhang Y, Chen P, Wen FF, Yuang B, Wang HG (2016) Fe_3O_4 nanospheres on MoS_2 nanoflake: Electrocatalysis and detection of Cr (VI) and nitrite. J Electroanal Chem 761:14–20

42. Sonkar PK, Ganesan V (2015) Synthesis and characterization of silver nanoparticle-anchored amine-functionalized mesoporous silica for electrocatalytic determination of nitrite. J Solid State Electrochem 19:2107–2115

43. Mani V, Wu TY, Chen SM (2014) Iron nanoparticles decorated graphene-multiwalled carbon nanotubes nanocomposite-modified glassy carbon electrode for the sensitive determination of nitrite. J Solid State Electrochem 18:1015–1023

44. Gligor D, Cuibus F, Peipmann R, Bund A (2017) Novel amperometric sensors for nitrite detection using electrodes modified with PEDOT prepared in ionic liquids. J Solid State Electrochem 21:281–290

45. Alamo LST, Tangkuaram T, Satienperakul S (2010) Determination of sulfite by pervaporation-flow injection with amperometric detection using copper hexacyanoferrate-carbon nanotube modified carbon paste electrode. Talanta 81:1793–1799